Carbon Nanotube with Chemically Bonded Graphene Leaves for Electronic and Optoelectronic Applications

ARTICLE *in* JOURNAL OF PHYSICAL CHEMISTRY LETTERS · JUNE 2011

Impact Factor: 7.46 · DOI: 10.1021/jz200641c

5 AUTHORS, INCLUDING:

Kehan Yu
Nanjing University of Posts and Telecommu…
51 PUBLICATIONS **1,625** CITATIONS
SEE PROFILE

Ganhua Lu
University of Wisconsin - Milwaukee
65 PUBLICATIONS **2,640** CITATIONS
SEE PROFILE

Zheng Bo
Zhejiang University
42 PUBLICATIONS **1,101** CITATIONS
SEE PROFILE

Shun Mao
University of Wisconsin - Milwaukee
85 PUBLICATIONS **2,382** CITATIONS
SEE PROFILE

THE JOURNAL OF PHYSICAL CHEMISTRY Letters

LETTER

pubs.acs.org/JPCL

Carbon Nanotube with Chemically Bonded Graphene Leaves for Electronic and Optoelectronic Applications

Kehan Yu,[†] Ganhua Lu,[†] Zheng Bo, Shun Mao, and Junhong Chen*

Department of Mechanical Engineering, University of Wisconsin-Milwaukee, Milwaukee, Wisconsin 53211, United States

Supporting Information

ABSTRACT: Hybrid nanomaterials composed of carbon nanotubes (CNTs) and graphene could potentially display outstanding properties that are superior to either CNTs or graphene alone. However, the inherent CNT−graphene loose junctions present in the CNT−graphene composites synthesized by existing methods significantly hinder the realization of the full potential held by CNT−graphene hybrids. In this letter, we report on a brand-new, three-dimensional (3D) carbon nanostructure comprising few-layer graphene (FLG) sheets inherently connected with CNTs through sp^2 carbons, resembling plant leaves (FLGs) growing on stems (CNTs). The resulting hybrid nanostructures were characterized using scanning electron microscopy, transmission electron microscopy (TEM), Raman spectroscopy, and X-ray photoelectron spectroscopy. The evolution of FLG sheets on CNTs was tracked by high-resolution TEM. Distinct from a random mixture of CNTs and graphene sheets (CNT+G) suffering from poor CNT−graphene contacts, our CNT−FLG structure has intrinsic chemical bonding between the two constituent components. We further show that the resulting CNT−FLG structure exhibits remarkable optoelectronic and gas sensing properties superior to its CNT or CNT+G counterparts. The new structure reported here is thus attractive for various electronic and optoelectronic applications.

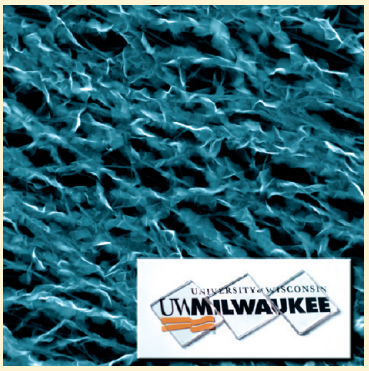

SECTION: Nanoparticles and Nanostructures

Combining carbon nanotubes (CNTs)[1] with graphene[2−5] has attracted increasing attention because the resulting hybrid CNT−graphene structures could potentially display outstanding properties that could not be attained by either component[6−10] alone. Recent modeling[11] and experimental evidence indicates that better isotropic thermal conductivity,[12] supercapacitors,[13,14] lithium-ion batteries,[15] and transparent conductive electrodes (TCEs)[16] can be achieved by CNT−graphene hybrids. However, the inherent CNT−graphene loose junctions (i.e., sheet resistance dominated by junctions) present in the CNT−graphene composites synthesized by existing methods significantly hinder the realization of the full potential held by CNT−graphene conjugates.

Existing methods to synthesize CNT−graphene composites include catalytic growth of CNTs between graphene oxide (GO) nanosheets,[13] layer-by-layer assembly of oppositely charged reduced GO (RGO) and CNTs,[17] or simple blending of CNTs and graphene.[15,16,18] Although these methods effectively diminished CNT−CNT junctions by adding graphene into CNT networks, additional new interfaces between the CNT and graphene/GO/RGO still unfavorably influence the functionality of CNT−graphene structures. Further enhanced properties can be anticipated for the resulting CNT−graphene structures if CNT−graphene junctions are eliminated by unifying the CNT with graphene by sp^2 carbons.

Here we show that few-layer graphene (FLG) sheets can be grown off and intrinsically connected with host multiwalled CNTs (MWCNTs) using plasma-enhanced chemical vapor deposition (PECVD) without deliberate introduction of catalysts. The host CNT and the as-grown FLG are inherently "fused" or chemically bonded together by sp^2 carbons, forming a single, total-carbon nanostructure with minimized CNT−graphene junctions. The growth mechanism of the CNT−FLG hybrid material was revealed by tracking specific sample locations during the graphene growth process using transmission electron microscopy (TEM). TCEs made of the novel CNT−FLG structure exhibit remarkable optoelectronic and gas sensing properties superior to its CNT counterpart.

Both planar CNT networks (randomly dispersed) and vertically aligned CNT arrays were used as hosts for the synthesis of CNT−FLG hybrid structures. Briefly, by using a catalyst-free PECVD technique, CNTs were first heated to 700 °C in an Ar flow (0.5 liter per minute or lpm) and then FLG was grown off CNTs at atmospheric pressure with CH_4 (0.5 lpm) as the carbon precursor (see details in the Experimental Section).[19] After the PECVD process, CNT−FLG hybrid structures were obtained with FLG (<10 nm thick) spreading off the host CNTs (Figure 1a,b; 1 min growth), in contrast to the smooth surface of pristine CNTs before the FLG growth (Figure S1, Supporting

Received: May 11, 2011
Accepted: June 6, 2011
Published: June 06, 2011

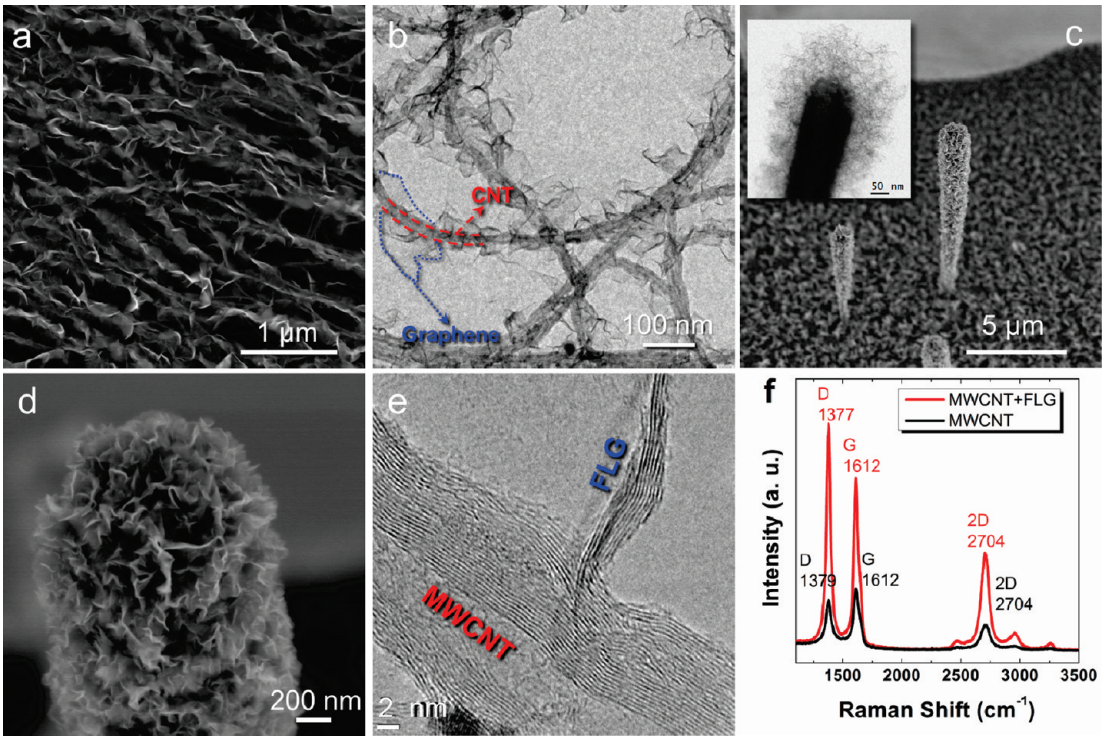

Figure 1. (a) SEM image of CNT−FLG hybrid structures. (b) TEM image of FLGs grown on CNTs suspended on a Cu TEM grid. (c) SEM image of FLGs grown on vertically aligned CNTs; the inset is a TEM image of the tip of a CNT−FLG, where the CNT stem (dark) is clearly distinguished from FLGs (bright). (d) A close view of the CNT−FLG tip in panel c. (e) HRTEM image of a CNT−FLG structure showing that the FLG is inherently bonded to the host CNT. (f) Raman spectra of pristine CNT (black) and CNT−FLG (red) films.

Information). The lateral dimension of the FLG typically ranged from 200 to 500 nm, which is consistent with a ∼300 nm/min growth rate previously observed and could be controlled by the growth time and the CH_4 concentration.[20] We also observed the swelling of CNT diameters after the PECVD. We carefully compared CNTs before and after PECVD and found more atomic carbon layers around the host CNTs (i.e., the number of walls increased for a MWCNT).

Similar FLG growth was also performed on vertically aligned CNTs. Figure 1c is a scanning electron microscopy (SEM) image showing that FLGs were grown on the entire external surface of every single vertical CNT. The inset of Figure 1c shows that, although the CNT stem was uniform in diameter, a much larger FLG corolla capped the tube tip, suggesting that the FLGs grew faster on the tip portion of a vertical CNT than on its lower portion. In a previous report we have demonstrated that the FLG growth rate depends on the local electric field; therefore, the rate of PECVD deposition is higher around a CNT tip (higher electric field), leading to more efficient FLG growth near the CNT tip.[21] Large FLG sheets with lateral dimensions of nearly 1 μm can be grown in some cases (Figure 1d).

The CNT−graphene interface has significant influence on the characteristics of the CNT−FLG hybrid structure. We used high-resolution TEM (HRTEM) to closely inspect the connecting domain between the host CNT and the FLG. Figure 1e is a representative HRTEM image that shows an FLG sheet growing directly off a host CNT; individual graphene layers of the FLG can be discerned. Moreover, the lattice fringes of the FLG match completely with those of the host CNT, suggesting that the graphitic lattice formation of the FLG initiated directly from the lattice of the CNT. The interlayer spacings for the CNT and the FLG in Figure 1e are measured as 0.346 and 0.348 nm, respectively, which are consistent with the interlayer distance of ∼0.34 nm for MWCNTs.[22,23] We examined many connecting areas between the CNT and the FLG for a number of CNT−FLG structures and obtained similar HRTEM results (see more HRTEM images in Figure S2, Supporting Information). The HRETM observations clearly indicate that, in our product CNT−FLG structures, the FLG and the host CNT are inherently bonded via sp^2 carbons. We note that fusing FLG with CNT into a single unified structure represents a giant step toward engineering interfaces between constituent components in hybrid nanostructures.

Raman spectroscopy was used to characterize CNT and CNT−FLG films supported on Si wafers (SEM image shown in Figure S3, Supporting Information). As shown in Figure 1f, the Raman spectrum of pristine CNTs (black curve) exhibits D, G, and 2D bands centered at 1379 cm^{-1}, 1612 cm^{-1}, and 2704 cm^{-1}, respectively. The corresponding D, G, and 2D bands of CNT−FLG (red curve) remained nearly at the same locations, suggesting very close chemical nature and electronic structure between the CNT and the CNT−FLG samples. The I_G/I_D ratio of pristine MWCNTs was 1.12, while the I_G/I_D ratio of CNT−FLG was 0.65. The disordered carbon in the CNT includes open-end carbon atoms and defects on the cylindrical carbon walls. Although the FLG is made of sp^2 carbons that should contribute to the G band signal, vacancies, grain boundaries, and open edges of the FLG may contribute considerably to the D band, resulting in a reduced I_G/I_D ratio.[24] The area ratio of 2D-to-G band I_{2D}/I_G of the CNT−FLG was 1.01, while the I_{2D}/I_G of the CNT was 0.71. The noteworthy increase in the I_{2D}/I_G ratio suggests the presence of more sp^2 carbon domains after the FLG growth.[25]

dx.doi.org/10.1021/jz200641c |J. Phys. Chem. Lett. 2011, 2, 1556–1562

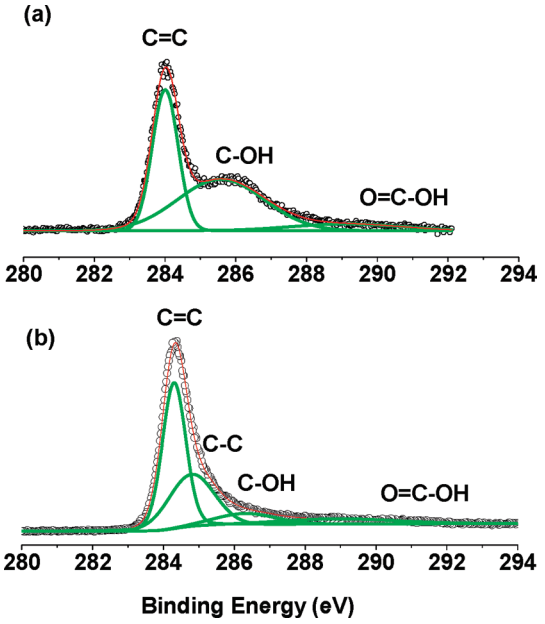

Figure 2. The C1s XPS spectra of MWCNT (a) and CNT−FLG (b). The raw data are presented by black circles, while the red curves are fitted. The peak components (green curves) were analyzed using Gaussian fit.

The evolution of disordered carbon from MWCNT to CNT−FLG was reflected in the X-ray photoelectron spectroscopy (XPS) spectrum as well (Figure 2). In the MWCNT, a significant C═C peak was derived from CNTs, but the C−C peak was very weak. Different from CNT−FLG, oxygen functional groups in the CNT sample originated from surfactants used to disperse CNTs (Figure 2a). The CNT−FLG contained C−C (32.6%), C−OH (9.3%), and O═C−OH (8.3%) (Figure 2b). During the PECVD process, surfactants were eliminated by high temperature and plasma. New C−OH and O═C−OH were introduced from the trace amount of water vapor involved in the synthesis. C−C was likely induced by defects and graphene sheet edge formation.

To elucidate the evolution from CNTs to CNT−FLG structures, we used TEM to track specified locations in two samples (A and B; prepared using home-grown and commercial CNTs, respectively) during the course of the FLG growth. Both samples went through the same PECVD process, except that Sample A was pretreated in Ar plasma (no carbon source) for 10 s prior to PECVD to study the influence of plasma treatment on the FLG growth. We found that this brief plasma treatment negligibly affected the final product because we obtained same CNT−FLG structures in both samples. Figure 3 presents micrographs from two locations (# 1: left column; # 2: middle and right columns) in Sample A at different processing stages (TEM results of more tracked areas in Samples A and B are respectively shown in Figures S4 and S5, Supporting Information). The external surfaces of starting CNTs are mostly smooth (Figure 3a,b). Figure 3c is an HRTEM image of the CNT squared in Figure 3b and clearly shows nine pairs of parallel dark lines corresponding with the (002) lattice image of the graphene sheets that build the CNT. Defects are inevitable in CVD-synthesized CNTs, even with optimized growth parameters.[26] Indeed, a few structural defects were apparent in the tube, which is in line with the existence of the D peak in the Raman spectrum from home-grown CNTs (Figure 1f).

After being treated in the Ar plasma for 10 s, the layout of the CNT network remained mostly unchanged (Figure 3d,e). However, the tube circled in Figure 3a was seen to break up after the plasma processing (Figure 3d), suggesting that the plasma treatment can generate more defects in CNTs. In Figure 3f, the CNT clearly had more topological defects than before plasma treatment (Figure 3c). Dai and co-workers have reported that CNTs can be unzipped to form graphene nanoribbons by Ar plasma etching (10 W) for as short as 10 s at a pressure of 40 mTorr.[27] Our plasma source had a lower power of ∼2.9 W and operated at atmospheric pressure. Thus, presumably, our plasma source could only create more defects in CNTs instead of completely opening them up. Note that no change in the CNT diameter was observed after the plasma processing.

FLG was successfully grown on the CNTs in Sample A after a 1 min PECVD process (Figure 3g,h). In addition to the formation of FLG, we also observed swelling of CNTs after the PECVD. We carefully compared the same CNT before (Figure 3c) and after (Figure 3i) the PECVD and found more layers of graphene around the host CNT (i.e., the number of walls increased in the CNT). The statistical analysis on the CNT diameter in Sample A revealed an increase of ∼3 nm for 1 min PECVD (Figure S6, Supporting Information). Small nanoparticles (NPs) likely from the precursor CNT sample were observed on the surface of CNT−FLG (Figure 3 and Figure S2, Supporting Information); however, they should have limited effect on the FLG growth that requires no catalysts.[20] Of course, these NPs may cause more defects when moving along the external surface of CNTs during the PECVD process, analogous to etching trenches in graphene with Fe NPs.[28]

The electron microscopy data shown here could provide important insights into the growth process of CNT−FLG structures. We can exclude the following two potential routes leading to such hybrid nanostructures: (1) FLG was first formed in the gas phase and then deposited on CNTs, through which sp^2 carbon-bonded CNT−FLG structure does not readily form; (2) FLG was formed by the plasma unzipping of starting CNTs. Unfolding a CNT of 10 nm in diameter along the tube axis will only result in a graphene sheet with a maximum width of ∼30 nm, whereas lateral sizes of product FLGs were typically above 100 nm and can be further increased by increasing the growth time. Therefore, our experimental observation suggests that FLG was grown off CNTs, i.e., FLG was chemically bonded to CNTs.

We propose the following growth process for hybrid CNT−FLG structures. The Ar plasma breaks the C−H bonds in CH_4 and provides carbon-containing radicals for the synthesis reaction. Simultaneously, plasma etching generates defects on CNT surfaces. These surface defects could serve as preferential nucleation sites to initiate the CVD growth of graphene (FLG), whereas the CNT itself could be a template for growing additional walls at a slower growth rate. As they could presumably grow faster at CNT defects than on the existing CNT walls, FLG sheets extend to free space, forming the graphene "leaves" of the CNT. Further investigation is warranted to better understand the CNT−FLG growth mechanism in the PECVD.

TCE films were fabricated on quartz slides using CNTs (before FLG growth), CNT−FLG structures (after FLG growth), and a random mixture of CNTs with graphene nanosheets (CNT+G, 3 wt % of G) to investigate the effect of FLG growth on the optoelectronic and electronic properties of the resulting TCE films. Figure 4a compares the transmittance (at λ = 550 nm) versus sheet resistance (R_S) for the aforementioned three types of

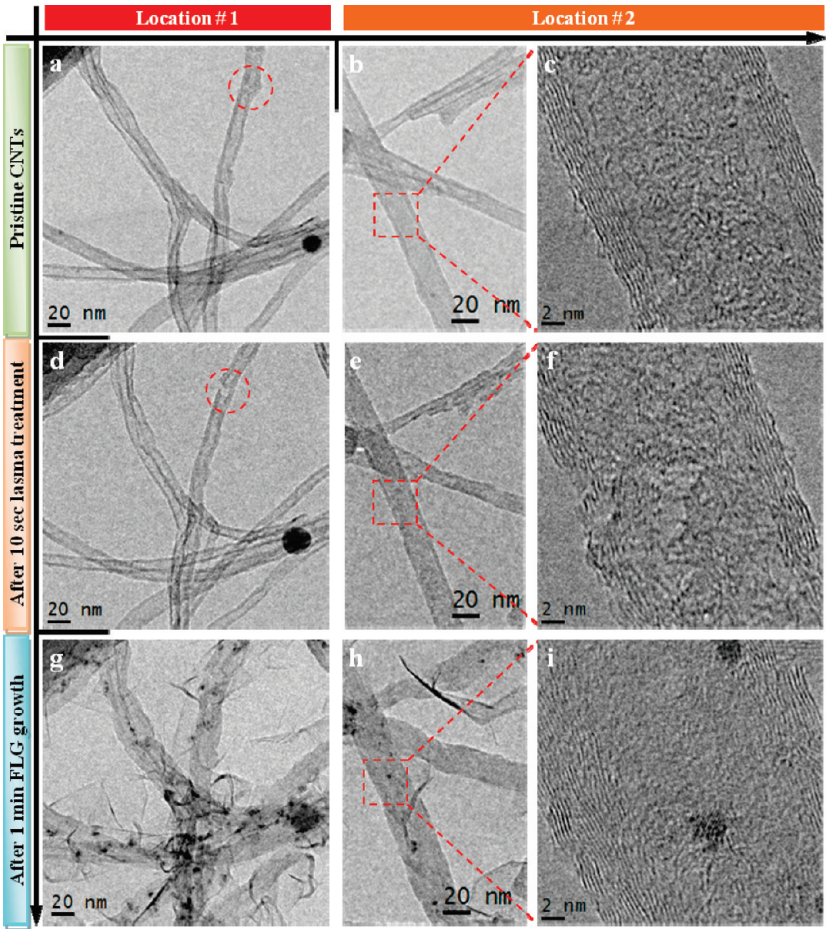

Figure 3. TEM and HRTEM (right column) images from two locations (Location 1: left column; Location 2: middle and right columns) in Sample A. (a−c) Pristine CNTs; (d−f) CNTs after being treated in Ar plasma for 10 s; (g−i) CNTs after a subsequent PECVD process for 1 min FLG growth.

films. It can be seen that R_S of the TCE dropped significantly for a given transmittance after the FLG growth. A highly transparent film with optical transmission of 90.4% at 550 nm and R_S of 12.5 kΩ/□ was obtained. In contrast, small addition of graphene nanosheets (PureSheets, NanoIntegris) into the CNT TCE film actually led to an increase in R_S, which is consistent with the literature as only an appropriate amount of RGO can lead to an decrease in R_S (3 wt % for single-walled CNTs).[18] Our sp^2-bonded CNT−FLG is also superior to the random mixture of CNT and RGO (transparency of 89%; $R_S \sim 15$ kΩ/□).[17] Therefore, the unified CNT−FLG structure significantly improves the electrical conductivity of TCEs without degrading the transparency likely through bridging loose tube−tube junctions. With more conductive paths present in a thin film through the direct growth of bonded graphene on CNTs, better electrical conductivity can be anticipated at a given transparency level. This is extremely attractive for high-transparency TCEs made of nanomaterials, in which percolation plays a key role in electrical conductivity. We note that both CNT and CNT+G TCEs exhibit lower slopes in the T% versus R_S plot than CNT−FLG (Figure 4a), suggesting a lower percolation threshold for CNT−FLG.[29]

Moreover, the growth of FLG can be used to repair damaged CNT films and restore electrical conductivity. We purposely scratched CNT TCE films to various degrees to demonstrate such a benefit. These damaged films were characterized by increased R_S to a value as high as 485 kΩ/□. After the FLG growth, all CNT TCE films showed consistent decrease in R_S with more damaged TCEs restored more significantly. As shown in Figure 4b, over a factor of 30 decrease in R_S can be achieved for the most damaged TCE.

The growth of FLG on CNTs also increased the surface area of the original CNT film, which is evidenced by various SEM and TEM images. This feature is attractive for sensing applications, particularly considering the excellent electrical contact between the CNT and the FLG in our structure. Figure 4c shows that the gas sensitivity S (defined as $(R_a - R_g)/R_a$, where R_a and R_g are the sensor resistance in air and target gas, respectively) of a CNT TCE increased by ~3 folds after the growth of FLG upon exposure to low concentration NO_2 (100 ppm) diluted in dry air. On the other hand, the addition of a small amount of random graphene sheets into a CNT film (CNT+G) did not improve the gas sensitivity at all (gray curve, Figure 4c). For molecular adsorption-based gas sensors (e.g., CNT and graphene sensors), the increase of surface area of active sensing materials introduces more electronic transfer between gas molecules and sensing materials, thereby leading to an enhanced sensing response. In addition, the diminishing junction resistance (R_j) could also help enhance the sensing performance of a CNT film because: (1) R_j dominates R_a ($R_a = R_{CNT} + R_j$ and normally $R_j \gg R_{CNT}$, where R_{CNT} is the intrinsic resistance of CNTs); (2) $(R_a - R_g)$ mostly depends on change in R_{CNT} because R_j changes negligibly upon gas exposure. After the FLG growth, R_j decreases significantly to

dx.doi.org/10.1021/jz200641c |J. Phys. Chem. Lett. 2011, 2, 1556–1562

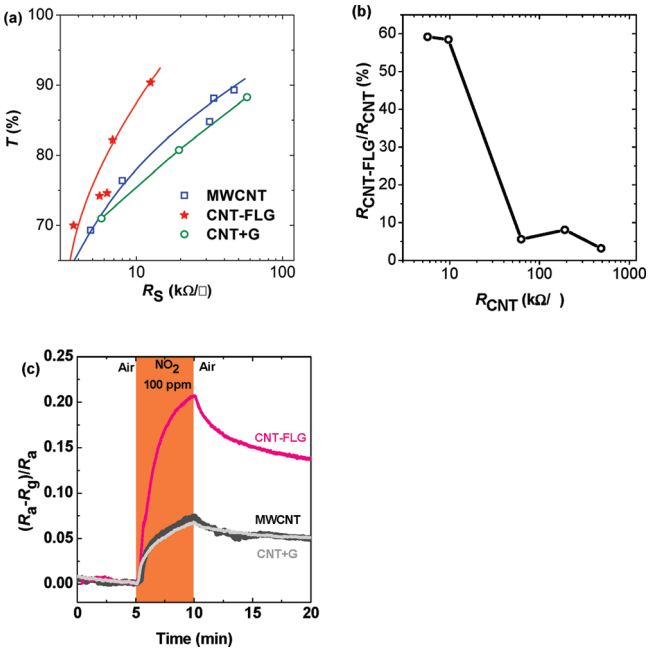

Figure 4. (a) Plot of transmittance (at λ = 550 nm) versus sheet resistance R_S for three different types of TCEs: MWCNT TCE before (□) and after (★) the FLG growth, and TCE based on random mixture of CNTs with graphene (○). The curves are guidelines for visual purposes only. (b) The sheet resistance change of damaged CNT TCE films after the FLG growth, normalized by the initial sheet resistance. (c) Sensing responses of CNT, CNT+G, and CNT−FLG TCE films against 100 ppm NO_2 diluted in dry air.

lower R_a, leading to an improved S. The random mixing of CNT with graphene did not lead to enhanced sensitivity simply because of the poor electrical contact between CNTs and graphene corresponding to poor charge transfer between the two components (Figure 4a). Clearly, a fused carbon structure is superior in gas sensing application due to both increased surface area and reduced junction resistance. It is interesting to note that the same film based on new CNT−FLG hybrid structures may be used simultaneously as a TCE and a gas sensor.

In summary, we have demonstrated a three-dimensional (3D) carbon hybrid nanostructure comprising FLGs inherently bonded to CNTs through sp^2 carbons. The CNT−FLG hybrid structures were synthesized using a catalyst-free, atmospheric pressure PECVD process. Unlike a random mixture of CNTs and graphene, the host CNT and the as-grown FLGs were intrinsically "fused" or bonded together by sp^2 carbons, forming a total-carbon nanostructure with minimized CNT−graphene junctions. The resulting CNT−FLG hybrid structures are attractive for various electronic and optoelectronic applications, as evidenced by significantly reduced sheet resistance and increased sensing response for a TCE based on such structures.

EXPERIMENTAL SECTION

CNT Sources. Three types of MWCNTs were used: home-grown CNTs, commercial CNTs, and vertically aligned CNT arrays. We used a 1″-tube furnace (Lindberg Blue, TF55035A-1) to synthesize CNTs through chemical vapor deposition (CVD). Briefly, thin films of Al (0.5 nm) and Fe (0.8 nm) were sequentially deposited onto a Si wafer as a diffusion barrier and a catalyst layer, respectively. C_2H_2 (0.05 lpm; bubbled through deionized (DI) water) and H_2 (0.5 lpm) served as carbon feedstock and carrier gas, respectively. The synthesis took place at 700 °C and under atmospheric pressure. As-grown CNTs were ∼10 nm in diameter and 300 μm in length. The commercial CNT powders were purchased from Alfa Aesar (20 nm O.D., 5−20 μm long). Vertically aligned CNTs (Nanolab Inc., diameter = 150 nm, length = 10 μm, site density = 2 × 10^6 tubes/cm^2) were grown on a silicon wafer with nickel catalysts by PECVD.[30] The inter-tube spacing was about 10 μm.

To form planar CNT networks, either the home-grown CNTs or commercial CNTs were first dispersed in ethanol by ultrasonication. Then, the CNT suspensions were drop-cast onto Cu TEM grids covered with lacey carbon film (Ted Pella) or Si wafers. CNTs were left on grids or wafers after ethanol evaporation.

Synthesis of CNT−FLG Structures by PECVD. CNT−FLG structures were produced using PECVD. The plasma reactor consists of a 1″ quartz tube that houses a tungsten needle cathode, a grounded graphite rod anode, and a direct current (dc) negative voltage supply (EMCO 4100N; up to −10 kV) to drive the dc plasma. Argon was used as the plasma gas. A tube furnace was used to heat up the reactor. The target samples (CNTs suspended on TEM grids, CNT thin films on quartz slides/Si wafers, or vertically aligned CNTs on Si wafers) were mounted on the top of the graphite rod. Prior to the growth, the reactor was heated to 700 °C and held at that temperature for 10 min in an Ar flow. The two discharge electrodes were separated by a distance of 1.0 cm. Then a CH_4 flow through a water bubbler was introduced into the reactor. Meanwhile, a dc plasma was initiated at a bias of 3.5 kV. The discharge current between the anode and the cathode was about 0.8 mA. Specifically, the Ar and CH_4 flow rates were 0.5 lpm and 0.5 lpm for CNT/TEM grid targets, and 1.0 lpm and 0.1 lpm for other targets. The growth period for TCEs was 2 min. At the end of the synthesis, the plasma was turned off while the system was cooled down to room temperature with a pure H_2 flow (1.0 lpm). Throughout the process, the reactor pressure was maintained at 1 atm.

Fabrication of TCEs. A vacuum filtration technique was adapted to make TCE films.[31] Commercial MWCNTs were ultrasonically dispersed in deionized (DI) water with assistance of surfactants (Alfa Aesar). Filter membranes made of 0.025 μm mixed cellulose ester (MCE, Millipore) were employed in a vacuum filtration apparatus. The solution was filtered down, and CNTs were caught on the membrane. Residual surfactant left in the film was subsequently washed away using purified water. The membrane with CNTs wetted with water was pressed against a quartz slide and then dried in an oven at 90 °C for 1 h. The MCE membrane was removed by acetone vapor bath and reflux condensation. The substrate/CNT/membrane assembly rested on a water-cooled condenser near the top of the container where distilled, condensing acetone continually washed the nanotube film. Product CNT TCEs were annealed in Ar flow (1 lpm) at 700 °C for 1 h. TCE films of CNT−FLG structures were obtained by PECVD processing of CNT films. Pure graphene suspension (PureSheets, research grade, NanoIntegris) with 3 wt % was added into the CNT suspension to fabricate the random CNT−graphene TCE film following the same procedure.

Characterization of CNT−FLG Structures. A field-emission SEM (Hitachi S 4800) was used to observe the morphology of CNTs and CNT−FLG structures; the SEM had a resolution of 1.4 nm at 1 kV acceleration voltage. TEM characterization of both CNTs and CNT−FLG structures was carried out using a

Hitachi H 9000 NAR TEM, which has a point resolution of 0.18 nm at 300 kV in the phase contrast HRTEM imaging mode. A location-tracked observation procedure previously used was employed to reveal the evolution from pristine CNTs to CNT−FLG structures.[32,33] In brief, several regions of CNTs on a TEM grid were identified and imaged prior to and after the plasma treatment or FLG growth experiments. A confocal Raman system, which is composed of a TRIAX 320 spectrograph, liquid nitrogen-cooled CCD (CCD 3000), and "spectrum one" CCD controller (all manufactured by HORIBA Jobin Yvon), was used to record the Raman spectra of samples with an excitation wavelength of 532 nm. XPS (Omicron ESCAprobe) was used to analyze the chemical composition and the nature of chemical bonds in the CNT−FLG materials. Gaussian fit was used to fit the XPS spectra with assistance of a free software (XPSPEAK, Chemistry, Chinese University of Hong Kong). Optical characterization of TCEs was conducted using a DT1000CE UV/vis light source (Analytical Instrument System, Inc.) and SD2000 fiber optic spectrometer (Ocean Optics, Inc.). Sheet resistance measurements on TCEs were accomplished by using the four point probe method. Gas sensing performance was based on two point probe measurements.

■ ASSOCIATED CONTENT

Supporting Information. Figure S1: additional SEM and TEM images of CNTs before and after FLG growth. Figure S2: TEM images showing that CNTs and FLG are inherently connected. Figure S3: SEM image of the CNT−FLG sample (on Si wafer) used for Raman analysis. Figures S4 and S5: additional TEM images tracking FLG growth on CNTs. Figure S6: Histograms of CNT diameters before and after FLG growth. This material is available free of charge via the Internet at http://pubs.acs.org.

■ AUTHOR INFORMATION

Corresponding Author

*E-mail: jhchen@uwm.edu.

Author Contributions

†These authors contributed equally.

■ ACKNOWLEDGMENT

This work was financially supported by the NSF (CMMI-0900509) and DOE (DE-EE0003208). TEM, SEM, XPS analyses, and sputtering depostion were performed in the UWM HRTEM Laboratory, UWM Electron Microscope Laboratory, Northwestern University Keck-II Center, and Argonne National Laboratary, respectively. We thank M. Gajdardziska-Josifovska for providing TEM access, D. Robertson for technical support with TEM, H. A. Owen for technical support with SEM, R. Arora for technical support with Raman, and X. Chen for technical support with XPS.

■ REFERENCES

(1) Iijima, S. Helical Microtubules of Graphitic Carbon. *Nature* **1991**, *354*, 56–58.

(2) Novoselov, K. S.; Geim, A. K.; Morozov, S. V.; Jiang, D.; Zhang, Y.; Dubonos, S. V.; Grigorieva, I. V.; Firsov, A. A. Electric Field Effect in Atomically Thin Carbon Films. *Science* **2004**, *306*, 666–669.

(3) Rao, C. N. R.; Sood, A. K.; Voggu, R.; Subrahmanyam, K. S. Some Novel Attributes of Graphene. *J. Phys. Chem. Lett.* **2010**, *1*, 572–580.

(4) Li, L.-s.; Yan, X. Colloidal Graphene Quantum Dots. *J. Phys. Chem. Lett.* **2010**, *1*, 2572–2576.

(5) Green, A. A.; Hersam, M. C. Emerging Methods for Producing Monodisperse Graphene Dispersions. *J. Phys. Chem. Lett.* **2010**, *1*, 544–549.

(6) Cao, Q.; Rogers, J. A. Ultrathin Films of Single-Walled Carbon Nanotubes for Electronics and Sensors: A Review of Fundamental and Applied Aspects. *Adv. Mater.* **2009**, *21*, 29–53.

(7) Geim, A. K.; Novoselov, K. S. The Rise of Graphene. *Nat. Mater.* **2007**, *6*, 183.

(8) Rao, C. N. R.; Sood, A. K.; Subrahmanyam, K. S.; Govindaraj, A. Graphene: The New Two-Dimensional Nanomaterial. *Angew. Chem., Int. Ed.* **2009**, *48*, 7752–7777.

(9) Dreyer, D. R.; Ruoff, R. S.; Bielawski, C. W. From Conception to Realization: An Historial Account of Graphene and Some Perspectives for Its Future. *Angew. Chem., Int. Ed.* **2010**, *49*, 9336–9344.

(10) Yang, W.; Ratinac, K. R.; Ringer, S. P.; Thordarson, P.; Gooding, J. J.; Braet, F. Carbon Nanomaterials in Biosensors: Should You Use Nanotubes or Graphene? *Angew. Chem., Int. Ed.* **2010**, *49*, 2114–2138.

(11) Shtogun, Y. V.; Woods, L. M. Many-Body van der Waals Interactions between Graphitic Nanostructures. *J. Phys. Chem. Lett.* **2010**, *1*, 1356–1362.

(12) Varshney, V.; Patnaik, S. S.; Roy, A. K.; Froudakis, G.; Farmer, B. L. Modeling of Thermal Transport in Pillared-Graphene Architectures. *ACS Nano* **2010**, *4*, 1153–1161.

(13) Fan, Z.; Yan, J.; Zhi, L.; Zhang, Q.; Wei, T.; Feng, J.; Zhang, M.; Qian, W.; Wei, F. A Three-Dimensional Carbon Nanotube/Graphene Sandwich and Its Application as Electrode in Supercapacitors. *Adv. Mater.* **2010**, *22*, 3723–3728.

(14) Yu, D.; Dai, L. Self-Assembled Graphene/Carbon Nanotube Hybrid Films for Supercapacitors. *J. Phys. Chem. Lett.* **2009**, *1*, 467–470.

(15) Yoo, E.; Kim, J.; Hosono, E.; Zhou, H. S.; Kudo, T.; Honma, I. Large Reversible Li Storage of Graphene Nanosheet Families for Use in Rechargeable Lithium Ion Batteries. *Nano Lett.* **2008**, *8*, 2277–2282.

(16) Tung, V. C.; Chen, L. M.; Allen, M. J.; Wassei, J. K.; Nelson, K.; Kaner, R. B.; Yang, Y. Low-Temperature Solution Processing of Graphene−Carbon Nanotube Hybrid Materials for High-Performance Transparent Conductors. *Nano Lett.* **2009**, *9*, 1949–1955.

(17) Hong, T. K.; Lee, D. W.; Choi, H. J.; Shin, H. S.; Kim, B. S. Transparent, Flexible Conducting Hybrid Multilayer Thin Films of Multiwalled Carbon Nanotubes with Graphene Nanosheets. *ACS Nano* **2010**, *4*, 3861–3868.

(18) King, P. J.; Khan, U.; Lotya, M.; De, S.; Coleman, J. N. Improvement of Transparent Conducting Nanotube Films by Addition of Small Quantities of Graphene. *ACS Nano* **2010**, *4*, 4238–4246.

(19) Yu, K.; Bo, Z.; Lu, G.; Mao, S.; Cui, S.; Zhu, Y.; Chen, X.; Ruoff, R. S.; Chen, J. Growth of Carbon Nanowalls at Atmospheric Pressure for One-Step Gas Sensor Fabrication. *Nanoscale Res. Lett.* **2011**, *6*, 202–210.

(20) Bo, Z.; Yu, K.; Lu, G.; Wang, P.; Mao, S.; Chen, J. Understanding Growth of Carbon Nanowalls at Atmospheric Pressure Using Normal Glow Discharge Plasma-Enhanced Chemical Vapor Deposition. *Carbon* **2011**, *49*, 1849–1858.

(21) Yu, K.; Wang, P.; Lu, G.; Chen, K.-H.; Bo, Z.; Chen, J. Patterning Vertically Oriented Graphene Sheets for Nanodevice Applications. *J. Phys. Chem. Lett.* **2011**, *2*, 537–542.

(22) Saito, Y.; Yoshikawa, T.; Bandow, S.; Tomita, M.; Hayashi, T. Interlayer Spacings in Carbon Nanotubes. *Phys. Rev. B* **1993**, *48*, 1907.

(23) Dresselhaus, M. S.; Dresselhaus, G.; Avouris, P. *Carbon Nanotubes: Synthesis, Structure, Properties, and Applications*; Springer Verlag: Berlin/Heidelberg/New York, 2001.

(24) Ferrari, A. C. Raman Spectroscopy of Graphene and Graphite: Disorder, Electron−Phonon Coupling, Doping and Nonadiabatic Effects. *Solid State Commun.* **2007**, *143*, 47–57.

(25) Ferrari, A. C.; Meyer, J. C.; Scardaci, V.; Casiraghi, C.; Lazzeri, M.; Mauri, F.; Piscanec, S.; Jiang, D.; Novoselov, K. S.; Roth, S.; et al.

Raman Spectrum of Graphene and Graphene Layers. *Phys. Rev. Lett.* **2006**, *97*, 187401, 187401-187404.

(26) Fan, Y.; Goldsmith, B. R.; Collins, P. G. Identifying and Counting Point Defects in Carbon Nanotubes. *Nat. Mater.* **2005**, *4*, 906–911.

(27) Jiao, L.; Zhang, L.; Wang, X.; Diankov, G.; Dai, H. Narrow Graphene Nanoribbons from Carbon Nanotubes. *Nature* **2009**, *458*, 877–880.

(28) Datta, S. S.; Strachan, D. R.; Khamis, S. M.; Johnson, A. T. C. Crystallographic Etching of Few-Layer Graphene. *Nano Lett.* **2008**, *8*, 1912–1915.

(29) De, S.; King, P. J.; Lyons, P. E.; Khan, U.; Coleman, J. N. Size Effects and the Problem with Percolation in Nanostructured Transparent Conductors. *ACS Nano* **2010**, *4*, 7064–7072.

(30) Huang, Z. P.; Xu, J. W.; Ren, Z. F.; Wang, J. H.; Siegal, M. P.; Provencio, P. N. Growth of Highly Oriented Carbon Nanotubes by Plasma-Enhanced Hot Filament Chemical Vapor Deposition. *Appl. Phys. Lett.* **1998**, *73*, 3845–3847.

(31) Wu, Z.; Chen, Z.; Du, X.; Logan, J. M.; Sippel, J.; Nikolou, M.; Kamaras, K.; Reynolds, J. R.; Tanner, D. B.; Hebard, A. F.; et al. Transparent, Conductive Carbon Nanotube Films. *Science* **2004**, *305*, 1273–1276.

(32) Zhu, L. Y.; Lu, G. H.; Mao, S.; Chen, J. H.; Dikin, D. A.; Chen, X. Q.; Ruoff, R. S. Ripening of Silver Nanoparticles on Carbon Nanotubes. *Nano* **2007**, *2*, 149–156.

(33) Lu, G. H.; Mao, S.; Park, S.; Ruoff, R. S.; Chen, J. H. Facile, Noncovalent Decoration of Graphene Oxide Sheets with Nanocrystals. *Nano Res.* **2009**, *2*, 192–200.